An overview of the QG-YBJ$^+$ model

Olivier Asselin

Scripps Institution of Oceanography, University of California San Diego, La Jolla, CA 90293-0213, USA

ABSTRACT

This document presents an overview of a numerical model for the two-way interaction of near-inertial waves with balanced eddies. Wave evolution is governed by the YBJ$^+$ equation (Asselin and Young 2019). The traditional quasigeostrophic equation dictates the evolution of potential vorticity, which includes the wave feedback term of Xie and Vanneste (2015). The model is pseudo-spectral in the horizontal and uses second-order finite differences to evaluate vertical and time derivatives. The code is available for download on Github.

1. Continuous problem

Let us consider a quasigeostrophic (QG) flow with weak vertical shear in the presence of near-inertial waves (NIWs). We assume that the evolution of the NIWs is dictated by the YBJ$^+$ equation (Asselin and Young 2019, 2020):

$$\mathsf{L}^+A_t + J(\psi,\mathsf{L}^+A) + \frac{i}{2}\mathsf{L}^+A\triangle\psi + \frac{if}{2}\triangle A = \nu\triangle^h\mathsf{L}^+A, \qquad (1)$$

where $J(a,b) \stackrel{\text{def}}{=} a_xb_y - a_yb_x$ is the horizontal Jacobian, $\triangle \stackrel{\text{def}}{=} \partial_x^2 + \partial_y^2$ is the horizontal Laplacian, ν is the diffusion coefficient and h is the hyperdiffusion order ($h = 1$ is regular Laplacian diffusion),

$$\mathsf{L} \stackrel{\text{def}}{=} \frac{\partial}{\partial z}\left(\frac{f^2}{N^2}\frac{\partial}{\partial z}\right), \qquad \mathsf{L}^+ \stackrel{\text{def}}{=} \mathsf{L} + \tfrac{1}{4}\triangle \qquad (2)$$

are frequently-occurring operators and the complex number A relates to the envelope of the leading-order wave fields:

$$u_0 + iv_0 = \mathrm{e}^{-ift}\mathsf{L}A, \qquad (3)$$

$$w_0 = -\frac{f^2}{N^2}\mathrm{e}^{-ift}(\partial_x - i\partial_y)A_z + \text{c.c.}, \qquad (4)$$

$$b_0 = if\mathrm{e}^{-ift}(\partial_x - i\partial_y)A_z + \text{c.c.}, \qquad (5)$$

$$p_0 = if\mathrm{e}^{-ift}(\partial_x - i\partial_y)A + \text{c.c.}, \qquad (6)$$

where c.c. stands for complex conjugate. We assume constant Coriolis frequency f. The base-state buoyancy $N(z)$ may have any depth dependence.

The Lagrangian-mean balanced flow evolves according to the traditional QG potential vorticity equation (Wagner and Young 2015)

$$q_t + J(\psi,q) = \nu_q\triangle^h q, \qquad (7)$$

where q is the potential vorticity and ψ the streamfunction. The NIWs feedback on the flow by modifying q-ψ relation (Xie and Vanneste 2015; Asselin and Young 2019):

$$q = \triangle\psi + \mathsf{L}\psi + \underbrace{\frac{i}{2f}J(\mathsf{L}^+A^*,\mathsf{L}^+A) + \frac{1}{4f}\triangle|\mathsf{L}^+A|^2}_{q^w}, \qquad (8)$$

where q^w is the wave feedback.

Boundary conditions

We assume that the flow is horizontally periodic and vertically bounded by rigid lids on which buoyancy is materially conserved:

$$\theta^\pm_t + J(\psi^\pm,\theta^\pm) = \nu_q\triangle^h\theta^\pm, \qquad (9)$$

where

$$\frac{f^2}{N^2}\psi_z \stackrel{\text{def}}{=} \theta(x,y,t) \qquad (10)$$

and the $\pm$ superscripts denote fields evaluated at the top and bottom boundaries, z^+ and z^-. We also require the vertical velocity of waves to vanish at the top and bottom, or from (4),

$$A^\pm_z = 0. \qquad (11)$$

Homogenous problem

The dynamic boundary conditions (9) can be simplified using Bretherton (1966)'s delta sheets of potential vorticity (see appendix for details). In this formulation, (7) to (9) are replaced with

$$q^H_t + J(\psi^H,q^H) = \nu_q\triangle^h q^H, \qquad (12)$$

$$q^H = \triangle\psi^H + \mathsf{L}\psi^H + q^w, \qquad (13)$$

where the homogeneous streamfunction ψ^H is identical to ψ at all interior points, but has zero vertical derivative at the top and bottom boundaries

$$\psi^H_z\Big|_{z^\pm} = 0, \tag{14}$$

and the homogenous potential vorticity q^H is modified by delta temperature sheets at the top and bottom,

$$q^H = q - \theta^+\delta(z - z^+) + \theta^-\delta(z - z^-). \tag{15}$$

For readability, we suppress the H superscripts, except in the appendix, where the homogeneous problem is explicitly discussed.

Integrating factor

Before treating the discretized problem, we note that diffusion can be integrated exactly using the integrating factor method,

$$\frac{\partial}{\partial t}\left(\hat{q}\,\mathrm{e}^{\nu_q k^{2h} t}\right) = \underbrace{-\widehat{J(\psi, q)}}_{\hat{F}_q}\,\mathrm{e}^{\nu_q k^{2h} t}, \tag{16}$$

$$\frac{\partial}{\partial t}\left(\hat{B}\mathrm{e}^{\nu k^{2h} t}\right) = \underbrace{\left(-\widehat{J(\psi, B)} - \tfrac{i}{2}\widehat{B\triangle\psi} + \tfrac{if}{2}k^2\hat{A}\right)}_{\hat{F}_B}\mathrm{e}^{\nu k^{2h} t}, \tag{17}$$

where hats decorate fields following a Fourier transform in the x and y directions with the horizontal wavenumber $k \stackrel{\text{def}}{=} \left(k_x^2 + k_y^2\right)^{1/2}$ and $B \stackrel{\text{def}}{=} \mathsf{L}^+A$. In what follows, we describe a numerical model that aims to solve to (16) and (17) with boundary conditions

$$\psi_z\Big|_{z^\pm} = A_z\Big|_{z^\pm} = 0. \tag{18}$$

2. Discretized problem

a. Variable representation

Let's now translate the continuous problem (16)-(18) into its discrete version. We first define the vertical grids on which to evaluate the variables:

$$z^u_i = i\Delta z, \quad z^s_i = (i - 1/2)\Delta z, \quad i = 1, 2, \ldots n_z, \tag{19}$$

where n_z is the number of grid points in the vertical, and the s and u superscripts denote the staggered and unstaggered grids. We place ψ, q, A and their even-order derivatives on the staggered grid, and their odd-order derivatives on the unstaggered grid (see Figure 1). For instance,

$$\psi_i \stackrel{\text{def}}{=} \psi(z^s_i), \quad \theta_i \stackrel{\text{def}}{=} \theta(z^u_i), \quad B_i \stackrel{\text{def}}{=} B(z^s_i). \tag{20}$$

Next, we expand the variables into Fourier series in the x and y directions; for instance,

$$\psi_i = \sum_{k_x=-n_x/2+1}^{n_x/2}\sum_{k_y=-n_y/2+1}^{n_y/2}\hat{\psi}_{k_x,k_y,i}\,\mathrm{e}^{i(k_x x + k_y y)}, \tag{21}$$

where k_x and k_y are the nondimensional wavenumbers (see section 3c) and n_x and n_y are the number of collocation grid points in the x and y directions. All variables are unstaggered in horizontal directions,

$$x_i = \Delta x(i-1), \quad y_i = \Delta y(i-1), \quad i = 1, 2, \ldots n_{x,y}. \tag{22}$$

Note that for any real-valued field, (21) is equal to its complex conjugate and $\hat{\psi}(-k_x, -k_y) = \hat{\psi}^*(k_x, k_y)$. This reality condition means that roughly half of the wavenumber components of $\hat{\psi}$ is redundant (except for mode $k_x = k_y = 0$). To save memory, the negative k_x values of k-space fields are not carried around, i.e. numerical arrays only comprise $k_x = 0, 1, 2, \ldots n_x/2$, and $k_y = -n_y/2 + 1, \ldots n_y/2 - 1$ (`kxa` and `kya` in the code). Furthermore, Fourier transforms happen in-place, meaning that the real-space and complex-valued Fourier-space versions of a variable occupy the same storage space. This requires a padding of the x dimension of real-space arrays with two extra spaces (i.e. `n1d=n1+2`).

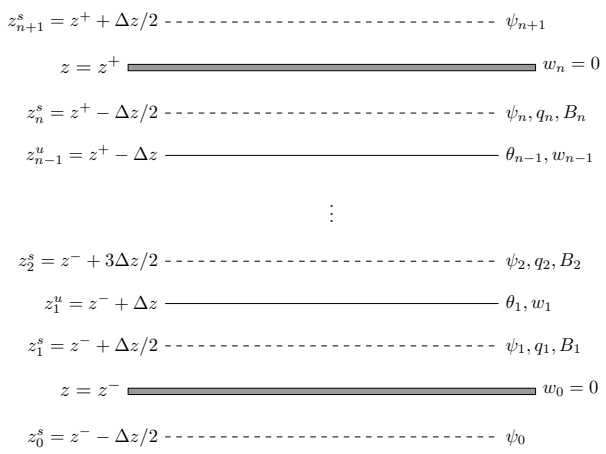

FIG. 1. Staggered (dashed) and unstaggered (solid) grids along with the ghost points, z^s_{n+1} and z^s_0.

b. Derivatives and nonlinear terms

Vertical and time derivatives are approximated using second order accurate centered finite differences (except for the first time step which uses Forward Euler; section 2c), and horizontal derivatives are spectral.

Nonlinear terms are computed via the transform method (see section 3a for details). As an illustration, consider the advective term $\widehat{\psi_x B_y}$. The transform method first involves computing the horizontal derivatives with spectral accuracy: $\widehat{\psi_x} = ik_x\hat{\psi}$, and $\widehat{B_y} = ik_y\hat{B}$. Then, we transform

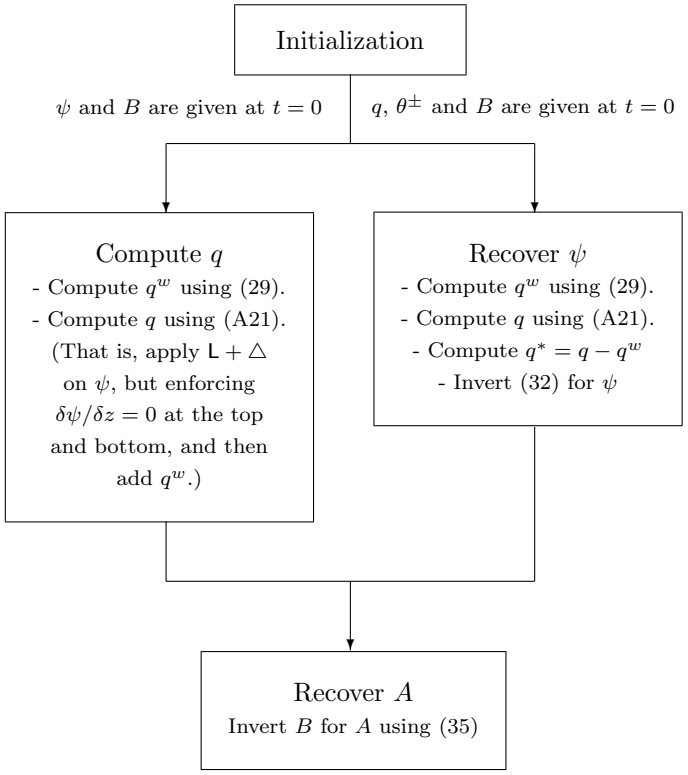

FIG. 2. Overview of the initialization procedure.

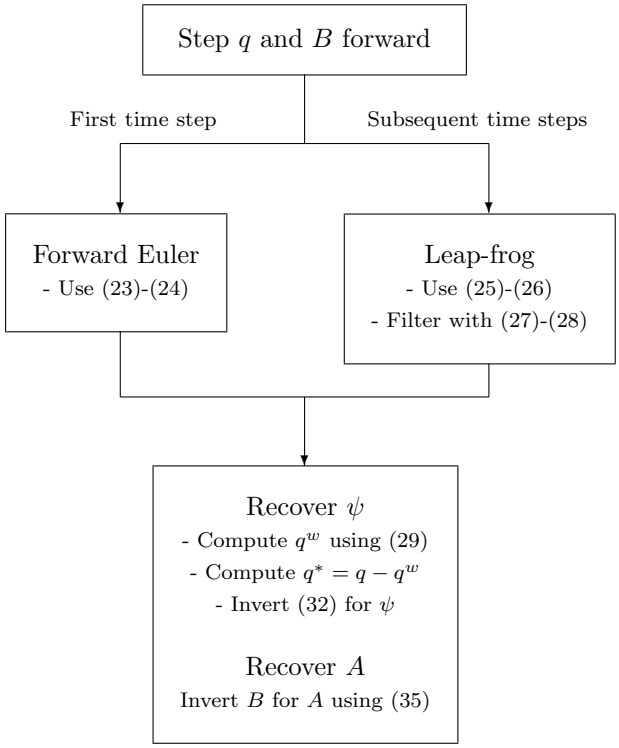

FIG. 3. Overview of the integration loop.

these fields back to real space using inverse fast fourier transforms, e.g. $\psi_x = \text{ifft}(ik_x\hat{\psi})$. Next, we multiply ψ_x with B_y in real-space. Finally, we transform the result back to Fourier space: $\widehat{\psi_x B_y} = \text{fft}(\psi_x B_y)$ and remove aliased wavenumbers using the 2/3 rule. Overall, this method implies $O(n \log n)$ operations rather than $O(n^2)$ for every horizontal dimension.

c. Overview of the integration procedure

The integration procedure is divided in three main steps: the initialization, the first time step, and the subsequent time steps. Figure 2 summarizes the initialization procedure for two different types of initial conditions. Following initialization comes time stepping (figure 3). For every wavenumber couple, (k_x, k_y), and every vertical level, i, we time-integrate the discretized version of the Fourier-space prognostic equations (16) and (17). For the first time step, we use the Forward Euler scheme,

$$\hat{q}^1 = \left(\hat{q}^0 + \Delta t \hat{F}_q^0\right) \mathrm{e}^{-\Delta t \nu_q k^{2h}}, \tag{23}$$

$$\hat{B}^1 = \left(\hat{B}^0 + \Delta t \hat{F}_B^0\right) \mathrm{e}^{-\Delta t \nu k^{2h}}, \tag{24}$$

where superscripts denote the time step, e.g., $\hat{B}^i = \hat{B}(t = i\Delta t)$. Vertical level subscripts have been omitted for clarity. For the subsequent time steps, we use the leap-frog scheme:

$$\hat{q}^{i+1} = \hat{q}^{i-1} \mathrm{e}^{-2\Delta t \nu_q k^{2h}} + 2\Delta t \hat{F}_q^i \mathrm{e}^{-\Delta t \nu_q k^{2h}}. \tag{25}$$

$$\hat{B}^{i+1} = \hat{B}^{i-1} \mathrm{e}^{-2\Delta t \nu k^{2h}} + 2\Delta t \hat{F}_B^i \mathrm{e}^{-\Delta t \nu k^{2h}}. \tag{26}$$

Then, to damp the computational mode, we filter the solution (Asselin 1972; Durran 2013):

$$\overline{\hat{B}^i} = \hat{B}^i + \gamma \left(\overline{\hat{B}^{i-1}} - 2\hat{B}^i + \hat{B}^{i+1}\right), \tag{27}$$

$$\overline{\hat{q}^i} = \hat{q}^i + \gamma \left(\overline{\hat{q}^{i-1}} - 2\hat{q}^i + \hat{q}^{i+1}\right), \tag{28}$$

where γ is a small damping parameter. The filter fields $\overline{\hat{q}^i}$ and $\overline{\hat{B}^i}$ respectively become $\hat{q}^{i-1}$ and $\hat{B}^{i-1}$ in (25) and (26) during the next time step.

d. Obtaining q^w

Once B is advanced to the new time step, we can compute the wave-averaged effects on potential vorticity, q^w, using the formula:

$$\hat{q}_i^w = \frac{i}{2f_0} J(\widehat{B_i^*, B_i}) - \frac{k^2}{4f_0} \widehat{B_i^* B_i}. \tag{29}$$

The nonlinear terms are evaluated using the transform method.

e. Obtaining ψ

Once q and q^w are known at the new time step, ψ is recovered using the discrete version of (13),

$$\hat{q}^* \stackrel{\text{def}}{=} \hat{q}_i - \hat{q}_i^w = -k^2\hat{\psi}_i + \frac{\delta}{\delta z}\left(\frac{f^2}{N^2}\frac{\delta\hat{\psi}_i}{\delta z}\right), \qquad (30)$$

with boundary conditions:

$$\left.\frac{\delta\hat{\psi}}{\delta z}\right|_{z^\pm} = 0, \qquad (31)$$

or $\hat{\psi}_0 = \hat{\psi}_1$ and $\hat{\psi}_{n+1} = \hat{\psi}_n$. This reduces to a simple tridiagonal system,

$$\begin{bmatrix}\hat{q}_1^*\\ \hat{q}_2^*\\ \hat{q}_3^*\\ \vdots\\ \hat{q}_i^*\\ \vdots\\ \hat{q}_N^*\end{bmatrix} = \begin{bmatrix}-(k^2+S_1) & S_1 & 0 & 0 & 0 & \dots & 0\\ S_1 & -(k^2+S_1+S_2) & S_2 & 0 & 0 & \dots & 0\\ 0 & S_2 & -(k^2+S_2+S_3) & S_3 & 0 & \dots & 0\\ \vdots & \ddots & \ddots & \ddots & \ddots & \vdots & \vdots\\ 0 & \dots & S_{i-1} & -(k^2+S_{i-1}+S_i) & S_i & \dots & 0\\ \vdots & \dots & \ddots & \ddots & \ddots & \ddots & \vdots\\ 0 & \dots & 0 & 0 & 0 & S_{N-1} & -(k^2+S_{N-1})\end{bmatrix}\begin{bmatrix}\hat{\psi}_1\\ \hat{\psi}_2\\ \hat{\psi}_3\\ \vdots\\ \hat{\psi}_i\\ \vdots\\ \hat{\psi}_N\end{bmatrix}, \qquad (32)$$

where $S_i = (f/(N(z_i^u)\Delta z)^2$. If $k = 0$, we may simply set $\hat{\psi} = 0$ since only derivatives of ψ matter in the dynamics of the system.

f. Obtaining A

Similarly, once B is known at the new time step, A is retrieved from B with

$$\hat{B}_i = \mathsf{L}^+\hat{A}_i = -\tfrac{1}{4}k^2\hat{A}_i + \frac{\delta}{\delta z}\left(\frac{f^2}{N^2}\frac{\delta\hat{A}_i}{\delta z}\right), \qquad (33)$$

given the boundary conditions,

$$\frac{\delta\hat{A}}{\delta z} = 0, \qquad (34)$$

or equivalently, $\hat{A}_0 = \hat{A}_1$ and $\hat{A}_{n+1} = \hat{A}_n$. This amounts to the tridiagonal system (32), except $q^* \to B$, $\psi \to A$ and $k^2 \to k^2/4$. Again, mode $k = 0$ of A may be set to zero since dispersion $\triangle A = 0$ for that mode. We are thus left with the tridiagonal matrix system

$$\begin{bmatrix}\hat{B}_1\\ \hat{B}_2\\ \vdots\\ \hat{B}_i\\ \vdots\\ \hat{B}_N\end{bmatrix} = \begin{bmatrix}-(\frac{1}{4}k^2+S_1) & S_1 & 0 & 0 & 0 & \dots & 0\\ S_1 & -(\frac{1}{4}k^2+S_1+S_2) & S_2 & 0 & 0 & \dots & 0\\ \vdots & \ddots & \ddots & \ddots & \ddots & \vdots & \vdots\\ 0 & \dots & S_{i-1} & -(\frac{1}{4}k^2+S_{i-1}+S_i) & S_i & \dots & 0\\ \vdots & \dots & \ddots & \ddots & \ddots & \ddots & \vdots\\ 0 & \dots & 0 & 0 & 0 & S_{N-1} & -(\frac{1}{4}k^2+S_{N-1})\end{bmatrix}\begin{bmatrix}\hat{A}_1\\ \hat{A}_2\\ \vdots\\ \hat{A}_i\\ \vdots\\ \hat{A}_N\end{bmatrix}. \qquad (35)$$

3. Details of implementation

a. The transform method and dealiasing

The nonlinear terms of this system have the generic form (in 1D)

$$\gamma(x) = \alpha(x)\beta(x), \qquad (36)$$

Such a quadratic nonlinear term amounts to a convolution sum in $k-$space:

$$\hat{\gamma}_k = \sum_{m+n=k}\hat{\alpha}_m\hat{\beta}_n, \qquad (37)$$

where the subscripts denote wavenumbers. A sum of the form (37) requires $O(N^2)$ operations in 1D, which becomes computationally prohibitive with a large number of grid points N. To overcome this issue, the *transform method* is

introduced. The trick is to

1. Compute the two terms in the convolution, $\hat{\alpha}_k$ and $\hat{\beta}_k$, in k-space,
2. Transform $[O(N \log N)]$ them to r-space to get $\alpha(x)$ and $\beta(x)$,
3. Perform the local multiplication $\gamma(x) = \alpha(x)\beta(x)$ in $r-$space at every grid point $[O(N)]$, then
4. Transform $[O(N \log N)]$ back the result to $k-$space to get $\hat{\gamma}_k$.

The whole procedure requires $O(N \log N)$ operations, which is much less than the brute force $O(N^2)$ at large resolution. The implementation, however, can lead to subtle errors. For a finite resolution, the field are represented with a finite number of wavenumbers:

$$\alpha_j = \sum_{m=-N/2}^{N/2-1} \hat{\alpha}_m e^{imx_j}, \quad \beta_j = \sum_{n=-N/2}^{N/2-1} \hat{\beta}_n e^{inx_j},$$

where x_j are the grid points, with $j = 0, 1, \ldots N-1$. In $r-$space, $\gamma_j = \alpha_j \beta_j$ so that

$$\begin{aligned} \hat{\gamma}_k &= \frac{1}{N} \sum_{j=0}^{N-1} \gamma_j e^{-ikx_j} \\ &= \frac{1}{N} \sum_{j=0}^{N-1} \left[\sum_{m=-N/2}^{N/2-1} \hat{\alpha}_m e^{imx_j} \sum_{n=-N/2}^{N/2-1} \hat{\beta}_n e^{inx_j} \right] e^{-ikx_j} \\ &= \sum_{m=-N/2}^{N/2-1} \sum_{n=-N/2}^{N/2-1} \hat{\alpha}_m \hat{\beta}_n \left[\frac{1}{N} \sum_{j=0}^{N-1} e^{i[(m+n)-k]x_j} \right] \end{aligned} \quad (38)$$

Orthogonality of the complex exponential basis functions guarantees

$$\frac{1}{N} \sum_{j=0}^{N-1} e^{ipx_j} = \begin{cases} 1 & \text{if } p = 0, \pm N, \pm 2N \ldots \\ 0 & \text{otherwise,} \end{cases} \quad (39)$$

such that the only terms surviving the previous sum are those satisfying $(m+n) - k = 0, \pm N, \pm 2N \ldots$ Since m, n and k can only take values from $-N/2$ to $N/2+1$, $(m+n)-k$ can only span values from $-3N/2+1$ to $3N/2-2$. The sum thus reduces to

$$\hat{\gamma}_k = \sum_{m+n=k} \hat{\alpha}_m \hat{\beta}_n + \sum_{m+n=k\pm N} \hat{\alpha}_m \hat{\beta}_n, \quad (40)$$

The first term is the exact solution (see (37)) and the second term is the *aliasing error*.

A simple way to get rid of this error is to cut all modes such that $k > N/3$. Indeed, if just before the second step (transform $\hat{\alpha}_k$ and $\hat{\beta}_k$ to r-space), k-space fields are truncated so that:

$$\hat{\alpha}_k = \begin{cases} \hat{\alpha} & \text{if } -N/3 \leq k \leq N/3 - 1 \\ 0 & \text{otherwise,} \end{cases} \quad (41)$$

(same thing with $\hat{\beta}$) then if the exact same steps (38) - (38) are performed, one now gets that m, n and k are in fact bounded by $-N/3$ and $N/3-1$, so that the worst case scenarios are:

$$\begin{aligned} -N < (-N/3 - N/3) - N/3 + 1 \leq (m+n) - k \\ \leq (N/3 - 1 + N/3 - 1) + N/3 < N, \end{aligned} \quad (42)$$

and the aliased term in (40) disappears. This dealiasing method is often called the 2/3 rule, since only keep only modes up to $k^{trunc} = 2k_{max}/3 = (2/3)(N/2) = N/3$. This method is readily generalized to multiple dimensions.

In the model, dealiasing is implemented by introducing a *dealiasing matrix* $L(k_x, k_y)$ with 0's at spurious modes, and 1's elsewhere. Spurious modes can be removed anytime by multiplying a $k-$space field by L. Furthermore, roughly half of the $k_x k_y$ area could be cut thanks to the reality condition $\hat{q}(-k_x, -k_y) = \hat{q}^*(k_x, k_y)$ for any real field q (with the exception of mode $k = 0$). To save storage space, negative k_x are also removed by multiplication of L, which is illustrated in figure 4.

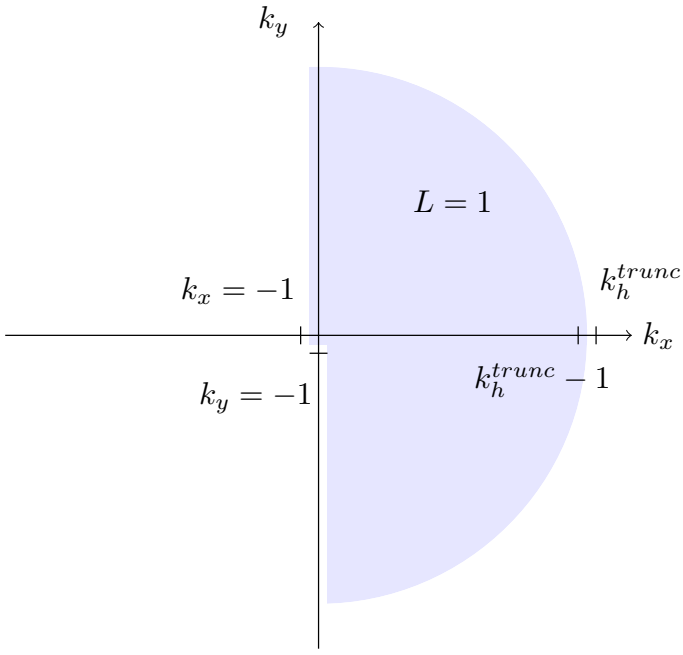

FIG. 4. Visual representation of modes cut (blank, $L = 0$) or preserved (shaded, $L = 1$) by the dealiasing matrix L.

b. Dealing with complex variables

In the original QG and Boussinesq models used in Asselin et al. (2016, 2018), all r-space variables are real. For instance, $\psi(\mathbf{x}), \mathbf{u}(\mathbf{x}) \in \mathbb{R}$. To minimize changes in the code's infrastructure, we decompose the newly-introduced complex r-space variables (A and B) into two real variables:

$$A(\mathbf{x}) = A^R(\mathbf{x}) + iA^I(\mathbf{x}), \qquad A^R, A^I \in \mathbb{R}, \tag{43}$$

$$B(\mathbf{x}) = B^R(\mathbf{x}) + iB^I(\mathbf{x}), \qquad B^R, B^I \in \mathbb{R}. \tag{44}$$

For instance we divide the YBJ$^+$ equation into its real and imaginary parts, and then take its Fourier transform:

$$\frac{\delta \hat{B}_i^R}{\delta t} = -J\widehat{(\psi_i, B_i^R)} - \frac{1}{2} f_0 k^2 \hat{A}_i^I + \frac{1}{2}\widehat{B_i^I \nabla^2 \psi_i}, \tag{45}$$

$$\frac{\delta \hat{B}_i^I}{\delta t} = -J\widehat{(\psi_i, B_i^I)} + \frac{1}{2} f_0 k^2 \hat{A}_i^R - \frac{1}{2}\widehat{B_i^R \nabla^2 \psi_i}. \tag{46}$$

The wave effect on potential vorticity can be written as:

$$\begin{aligned}\hat{q}^w &= \frac{i}{2f} J\widehat{(B^*, B)} + \frac{1}{4f}\widehat{\nabla^2 |B|^2} \\ &= \frac{1}{f}\left(\widehat{B_y^R B_x^I} - \widehat{B_x^R B_y^I}\right) - \frac{k^2}{4f}\left(\widehat{B^R B^R} + \widehat{B^I B^I}\right). \end{aligned} \tag{47}$$

c. Dimensionless equations

The numerical model integrates the equations in their nondimensional form:

$$(x, y) = L(x', y'), \quad z = Hz', \quad t = (L/U)t' \tag{48}$$

$$(u, v) = U(u', v'), \quad (\tilde{u}, \tilde{v}) = \tilde{U}(\tilde{u}', \tilde{v}'), \tag{49}$$

$$B = \tilde{U} B', \qquad A = \tilde{U} L^2 \mathrm{Bu} A' \tag{50}$$

where primes denote nondimensional variables. Note that we assumed the flow and the wave envelope to share the same length and time scales, but potentially different amplitudes. With these assumptions, we can write down the nondimensional potential vorticity:

$$q' = \triangle \psi' + \mathrm{Bu}^{-1} \mathsf{L}\psi' + \mathrm{Ro}\frac{\tilde{U}^2}{U^2}\left[\frac{i}{2} J(B'^*, B') + \frac{1}{4}\triangle |B'|^2\right], \tag{51}$$

where $\mathrm{Bu}^{-1} = (fL/N_0 H)^2$ is the inverse Burger number (disclaimer: in the code, `Bu` is Bu^{-1} here) and $\mathrm{Ro} = U/fL$ is the (flow) Rossby number. The nondimensional QG and YBJ$^+$ equations are

$$q'_t + J(\psi', q') = 0, \tag{52}$$

$$B'_t + J(\psi', B') + \frac{i}{2} B' \nabla^2 \psi' + \frac{\mathrm{Bu}}{\mathrm{Ro}} \frac{i}{2} \nabla^2 A' = 0. \tag{53}$$

Computations are sped up with a nondimensional domain size of $(2\pi)^3$, because then wavenumbers are integers.

d. Parallelization

The model is designed to perform parallellized computations via MPI. The transform method requires frequent Fourier transforms in both horizontal directions. These operations require that a given processor holds all horizontal vectors (k_x, k_y) at a given height, z_i. For most of the integration procedure, fields are thus parallelized along z. An exception, examined below, is the inversion of q for ψ and B for A, during which the fields are parallelized along k_y.

To minimize costly communication between processors, some vertical levels, called *halos*, are carried by more than one processor (see Figure 5). The number of vertical derivatives to be performed on a field variables determines how many halo levels are needed. Therefore, arrays representing different variables will have different z dimensions, as shown in Table 1.

Variables	Halo level
U, V	2
ψ, q	1
B, A	0

TABLE 1. Some variables and their halo levels.

To obtain ψ and A, we must solve elliptic equations in z for each wavevector (k_x, k_y), i.e. (30) and (33). This requires that a given processor holds, for a given wavevector, all vertical levels. Therefore, in order to solve the matrix systems (32) and (35), we need to *transpose* data so that it is parallelized along another dimension, here set to be k_y.

The subroutine `mpi_transpose` allows to switch the parallelization axis of a given field. For instance, after computing the right-hand side of the elliptic equation, call it $\hat{F}(k_x, k_y, z^p)$, where the p superscript denotes parallelization along this dimension, we can transpose it so that it is parallelized along k_y instead of z, yielding $\hat{F}^T(k_x, z, k_y^p)$. In general, the initial $\phi(d_1, d_2, d_3^p)$ and final $\phi_T(d_1, d_3, d_2^p)$ setups for a transpose are as illustrated in figure 6.

APPENDIX

The treatment of inhomogeneous boundary conditions in the q-ψ inversion problem

The continuous problem

Let us consider a quasigeostrophic flow with arbitrary buoyancy distribution of its top and bottom boundaries:

$$q = \nabla^2 \psi + \left(\frac{f^2}{N^2}\psi_z\right)_z, \qquad z^- \le z \le z^+, \tag{A1}$$

$$\frac{f^2}{N^2}\psi_z = \theta^{\pm}(x, y, t), \qquad z = z^{\pm}. \tag{A2}$$

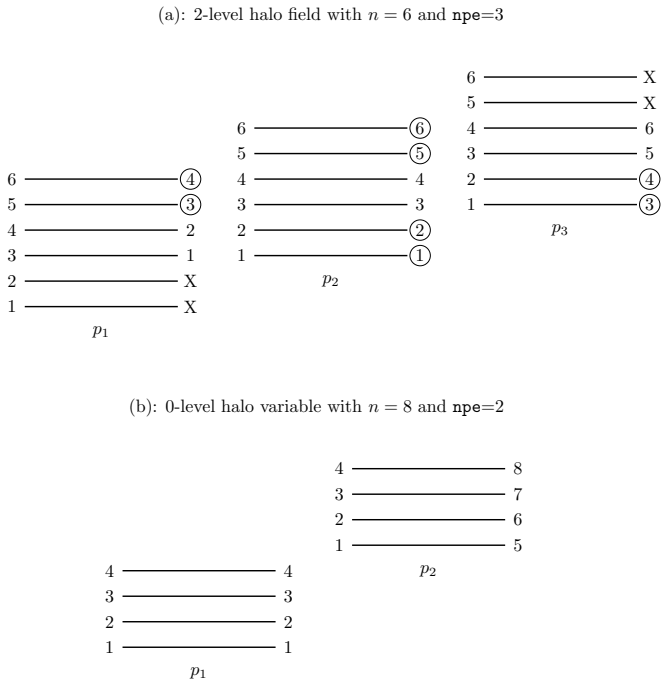

FIG. 5. Examples of the vertical array configurations. The horizontal lines represent vertical levels for each processor p_i. On the left side of each level we have the array index corresponding to the actual associated $z-$level on the right. X-marked regions are insignificant and padded with 0's. Circled $z-$levels are halos.

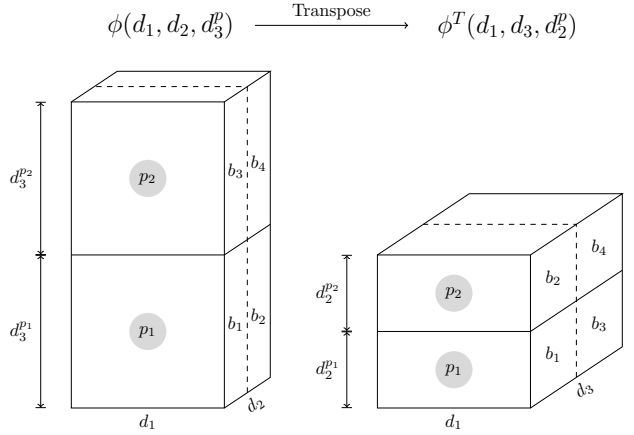

FIG. 6. Illustration of the initial and final multidimensional array setups for a transpose. Data is here divided by the solid lines, that is, amongst 2 processes. Initially, ϕ is parallelized along dimension d_3, whereas the transposed field ϕ^T is parallelized along d_2, as denoted by the p superscripts. Notice that after the transpose, the scond and third dimensions were swapped. Furthermore, the dashed lines bound the 4 data blocks that are temporarily written on scratch arrays for send and receive buffers.

1

Without loss of generality, wave feedback is removed from (A1). Following Bretherton (1966), we convert the inhomogeneous boundary conditions into delta Dirac sheets of potential vorticity just above the bottom and below the top. To do so, we first decompose the streamfunction into

$$\psi = \psi^H + a^+(z)\theta^+(x,y,t) - a^-(z)\theta^-(x,y,t), \qquad \text{(A3)}$$

and impose:

$$\frac{f^2}{N^2}\psi^H_z\Big|_{z=z^\pm} = 0 \qquad \frac{f^2}{N^2}a^\pm_z\Big|_{z=z^\mp} = 0 \qquad \text{(A4)}$$

$$\frac{f^2}{N^2}a^+_z\Big|_{z=z^+} = 1 \qquad \frac{f^2}{N^2}a^-_z\Big|_{z=z^-} = -1. \qquad \text{(A5)}$$

Simply put, ψ^H solutions the homogeneous problem and $a^\pm$ guarantees the satisfaction of the inhomogeneous boundary conditions. There are many valid choices for $a^\pm$; we pick

$$\frac{f^2}{N^2}a^+_z = \Theta(z - (z^+ - \epsilon)), \qquad \text{(A6)}$$

$$\frac{f^2}{N^2}a^-_z = \Theta(z - (z^- + \epsilon)) - 1, \qquad \text{(A7)}$$

where Θ is the Heaviside step function and ϵ is a small parameter. As a result,

$$a^+ = \int_{z^-}^{z} \frac{N^2}{f^2}\Theta(z' - (z^+ - \epsilon))dz' \qquad \text{(A8)}$$

$$a^- = \int_{z^-}^{z} \frac{N^2}{f^2}\left[\Theta(z' - (z^- + \epsilon)) - 1\right]dz' \qquad \text{(A9)}$$

Since ϵ is small,

$$a^+ = \begin{cases} +\epsilon N^2(z^+)/f^2 & \text{if } z^+ - \epsilon < z \le z^+, \\ 0 & \text{otherwise,} \end{cases} \qquad \text{(A10)}$$

$$a^- = \begin{cases} -\epsilon N^2(z^-)/f^2 & \text{if } z^- \le z < z^- + \epsilon, \\ 0 & \text{otherwise.} \end{cases} \qquad \text{(A11)}$$

Simply put, the $a^\pm$ contributions to the streamfunction (A3) vanish as $\epsilon \to 0$ while the satisfaction of the boundary conditions (A4)-(A5) is maintained. Inserting (A3) into the potential vorticity equation (A1) yields

$$\begin{aligned} q &= \nabla^2\psi^H + \left(\frac{f^2}{N^2}\psi^H_z\right)_z + \underbrace{a^+\nabla^2\theta^+ - a^-\nabla^2\theta^-}_{O(\epsilon)} \\ &\quad + \theta^+\delta(z - z^+ + \epsilon) - \theta^-\delta(z - z^- - \epsilon), \end{aligned} \qquad \text{(A12)}$$

where δ is the Dirac delta function. Here again, the $a^\pm$ terms vanish as $\epsilon \to 0$. As such, the initial problem (A1)-(A2) may be reformulated as:

$$q^H = \nabla^2\psi^H + \left(\frac{f^2}{N^2}\psi^H_z\right)_z, \qquad z^- \le z \le z^+, \qquad \text{(A13)}$$

with the homogeneous boundary conditions,

$$\frac{f^2}{N^2}\psi_z^H\Big|_{z=z^\pm} = 0, \tag{A14}$$

where potential vorticity is now modified by delta sheets near the top and bottom boundaries:

$$q^H = q - \theta^+\delta(z - z^+ + \epsilon) + \theta^-\delta(z - z^- - \epsilon). \tag{A15}$$

The discrete problem

A finite-difference version of the above trick may also be implemented. The corresponding $a_i^\pm$ are defined on staggered grid points, $z_i^s = (i - 1/2)\Delta z$,

$$a_i^+ = \begin{cases} +2(z_i - z^+)N^2(z^+)/f^2 & \text{if } z_i > z^+, \\ 0 & \text{otherwise,} \end{cases} \tag{A16}$$

$$a_i^- = \begin{cases} -2(z_i - z^-)N^2(z^-)/f^2 & \text{if } z_i < z^-, \\ 0 & \text{otherwise.} \end{cases} \tag{A17}$$

Note that the discretized $a_i^\pm$ are zero everywhere at interior grid points, but nonzero at the ghost grid points, z_{N+1} and z_0. By construction,

$$\frac{f^2}{N^2}\frac{\delta\psi^H}{\delta z}\Big|_{z=z^\pm} = 0, \tag{A18}$$

and one can confirm that

$$\begin{aligned}\frac{f^2}{N^2}\frac{\delta a^+}{\delta z}\Big|_{z=z^+} &= \frac{f^2}{N^2(z^+)}\frac{a^+(z^+ + \Delta z/2) - a^+(z^+ - \Delta z/2)}{\Delta z} \\ &= \frac{f^2}{N^2(z^+)}\frac{\Delta z N^2(z^+)/f^2 - 0}{\Delta z} = 1, \end{aligned} \tag{A19}$$

$$\begin{aligned}\frac{f^2}{N^2}\frac{\delta a^-}{\delta z}\Big|_{z=z^-} &= \frac{f^2}{N^2(z^-)}\frac{a^-(z^- + \Delta z/2) - a^-(z^- - \Delta z/2)}{\Delta z} \\ &= \frac{f^2}{N^2(z^-)}\frac{0 - \Delta z N^2(z^-)/f^2}{\Delta z} = -1, \end{aligned} \tag{A20}$$

where $\delta/\delta z$ denotes the second-order centered finite-difference operator. Then, the discretized potential vorticity equation (A12) can be written as:

$$q_i^H = q_i - \frac{\theta^+ - \theta^-}{\Delta z} = \nabla^2\psi_i^H + \frac{\delta}{\delta z}\left(\frac{f^2}{N^2}\frac{\delta\psi_i^H}{\delta z}\right). \tag{A21}$$

Interestingly, the $\theta^\pm$ terms precisely cancel the corresponding terms in q_N and q_1. As such, there is no need to keep track of $\theta^\pm$. Instead, one may simply use the initial $\psi(t = 0)$ to compute q_i^H using (A21). That is, we use $\psi_i^H = \psi_i$ except that $\delta\psi_i^H/\delta z$ is forced to zero at the top and bottom boundaries. This generates a potential vorticity field modified with a discretized version of Bretherton's delta sheets ($1/\Delta z$ instead of δ).

The uninitiated reader may find it counter-intuitive that the temperature conditions are not necessary in this formulation of the problem. This tension can be reconciled by realizing that the temperature equation, (9), can be expressed as:

$$\begin{aligned}\theta_t^+ &= -J(\psi^+, \theta^+) \\ &= -J(\frac{\psi_n + \psi_{n+1}}{2}, \theta^+) \\ &= -J(\psi_n + \frac{\Delta z}{2}\theta^+, \theta^+) \\ &= -J(\psi_n, \theta^+). \end{aligned} \tag{A22}$$

Therefore, advecting buoyancy at the top is equivalent to advecting it using the streamfunction at the top staggered grid point, $\Delta z/2$ below the top, or precisely where q_n is advected. That is, the advection of q^H at its top and bottom implicitly incorporates the advection of $\theta^\pm$.

REFERENCES

Asselin, O., P. Bartello, and D. N. Straub, 2016: On quasigeostrophic dynamics near the tropopause. *Physics of Fluids*, **28 (2)**, 026 601.

Asselin, O., P. Bartello, and D. N. Straub, 2018: On boussinesq dynamics near the tropopause. *Journal of the Atmospheric Sciences*, **75 (2)**, 571–585.

Asselin, O. and W. R. Young, 2019: An improved model of near-inertial wave dynamics. *Journal of Fluid Mechanics*, **876**, 428–448.

Asselin, O. and W. R. Young, 2020: Penetration of wind-generated near-inertial waves into a turbulent ocean. *arXiv preprint arXiv:1912.08323*.

Asselin, R., 1972: Frequency filter for time integrations. *Mon. Wea. Rev*, **100 (6)**, 487–490.

Bretherton, F. P., 1966: Critical layer instability in baroclinic flows. *Quarterly Journal of the Royal Meteorological Society*, **92 (393)**, 325–334.

Durran, D. R., 2013: *Numerical Methods for Wave Equations in Geophysical Fluid Dynamics*, Vol. 32. Springer Science & Business Media.

Wagner, G. L. and W. R. Young, 2015: Available potential vorticity and wave-averaged quasi-geostrophic flow. *Journal of Fluid Mechanics*, **785**, 401–424.

Xie, J.-H. and J. Vanneste, 2015: A generalised-lagrangian-mean model of the interactions between near-inertial waves and mean flow. *Journal of Fluid Mechanics*, **774**, 143–169.